**The response of ozone deposition to heat and dry anomalies – roles of non-stomatal deposition**

**A. Y. H. Wong[1], J. A. Geddes[1], J. A. Ducker[2], C. D. Holmes[2], S. Fares[3,4], A. H. Goldstein[5,6], I. Mammarella[7], J. W. Munger[8]**

[1]Deparment of Earth and Environment, Boston University, Boston, Massachusetts, USA

[2]Department of Earth, Ocean and Atmospheric Science, Florida State University, Tallahassee, Florida, USA

[3]Council of Agricultural Research and Economics, Research Centre of Forestry and Wood, Rome, Italy

[4]National Research Council, Institute of Bioeconomy, Rome, Italy

[5]Department of Environmental Science, Policy, and Management, University of California, Berkeley, California, USA

[6]Department of Civil and Environmental Engineering, University of California, Berkeley, California, USA

[7]Institute of Atmospheric and Earth System Research/Physics, University of Helsinki, Helsinki, Finland

[8]School of Engineering and Applied Science and Department of Earth and Planetary Sciences, Harvard University, Cambridge, Massachusetts, USA

**Contents of this file**

**Introduction**

This supporting information contains the methods of evapotranspiration partitioning, inferring canopy stomatal conductance, the main characteristics of the sites and a brief description of the dry deposition model used.

**Text S1.**

We use two different methods to estimate the transpiration component of total latent heat flux:

1) The simple approach assume that 10% and 20% of the latent heat flux are attributable to soil evaporation at *Ha* and *Hyy*, respectively (Ducker et al., 2018). When evaporation from wet surface was likely, as indicated by precipitation (cumulative precipitation > 0.2 mm) within 12 hours or possibility of dew presence (RH > 80%). In addition, we exclude $g_{s,w}$ values that are probably unrealistic ($g_{s,w}$ > 5 cm s$^{-1}$ or $g_{s,w}$ < 0), $g_s$ data point are excluded. This approach is consistent with previous work on ozone deposition (Clifton et al., 2017; Fares et al., 2010; Kurpius & Goldstein, 2003).

2) The approach used in the main text is based on the recent work of Nelson et al. (2018), which is based on the theory of water use efficiency (WUE) and considers both water and carbon fluxes. Here we give a brief outline to the method. Filtering out the time period when surface is likely to be wet, and therefore contributing to evaporation (*E*), we obtain the time periods when transpiration (*T*) is like to dominate evapotranspiration (*ET*), which is directly measured as latent heat flux. Over these time periods, WUE, which is defined as GPP/*T*, can be approximated as GPP/*ET*. Then a machine learning method, Random Forest Regressor (RFR) (Breiman, 2001), is applied to modelled the relationship between WUE and environmental variable. The RFR-modelled WUE (WUE$_{pred}$) is then used to back-infer *T*:

$$T = \frac{GPP}{WUE_{pred}} \quad (S1)$$

The details of data filtering and predictors of RFR can be found in Nelson et al. (2018). Stoy et al. (2019) state this class of methods assumes *T* = *ET* intermittently, which is a good assumption for ecosystems with high LAI. Otherwise *T* can be overestimated.

**Text S2.**

Calculations of aerodynamic, laminar boundary layer, and stomatal resistance follow the methods of Ducker et al. (2018) and are repeated here for clarity. The evaporative-resistive framework of Penman-Montieth inversion (Gerosa et al., 2007) is given as follow:

$$r_{s,w} = \frac{1}{g_{s,w}} = \left(\frac{0.622\rho}{P}\frac{e_s(T_{can})-e}{T}\right) - r_{a,w} - r_{b,w} \text{ (S2)}$$

Where $r_{a,w}$, $r_{b,w}$, $r_{s,w}$, $g_{s,w}$, are the aerodynamic, laminar boundary layer and stomatal resistance (s m$^{-1}$) and stomatal conductance (m s$^{-1}$) of water vapor, and $\rho$ (kg m$^{-3}$), $P$ (Pa) is air density and pressure, and $e_s(T_{can})$, $e$ and $T$ are saturated water vapor pressure at canopy temperature ($T_{can}$, K) and water vapor pressure at measurement height (Pa) and transpiration flux (kg m$^{-2}$ s$^{-1}$), respectively. $T_{can}$ is estimated as:

$$T_{can} = T_a + \frac{H}{\rho c_p}(r_{a,H} + r_{b,H}) \text{ (S3)}$$

where $T_a$ (K), $H$ (W m$^{-2}$) and $c_p$ (J kg$^{-1}$ K$^{-1}$) are air temperature at measurement height, sensible heat flux and specific heat of air at constant pressure, and $r_{a,H}$ and $r_{b,H}$ are the aerodynamic and laminar boundary-layer resistance of heat. Assuming $r_{a,H} = r_{a,w}$ , and applying Monin-Obukhov Similarity Theory (Foken, 2006; Monin & Obukhov, 1954), $r_a$ is calculated as:

$$r_a = \frac{1}{ku_*}(\ln\frac{z-d}{z_0} - \psi\left(\frac{z-d}{L}\right) + \psi\left(\frac{z_0}{L}\right)) \text{ (S4)}$$

where $k$ is the von Karman Constant, $u_*$ (m s$^{-1}$) is friction velocity, $z$, $z_0$ and $d$ are measurement height, roughness length and displacement height (m). We take $z_0 = 0.1$ $h_c$ and $d = 0.7$ $h_c$, where $h_c$ is canopy height (Ducker et al., 2018). Obukhov Length ($L$) is expanded to measurable quantities:

$$L = -\frac{u_*^3 T_v}{kgQ_{v0}} = -\frac{u_*^3 \rho c_p \theta(1+0.61q)}{kg(H(1+0.61q)+0.61c_p\theta E)} \text{ (S5)}$$

where $q$, $\theta$, $g$, $E$ are absolute humidity (kg kg$^{-1}$), potential temperature (K), gravitational acceleration (m s$^{-2}$) and total evaporative flux (kg m$^{-2}$ s$^{-1}$). The stability function $\psi$ takes the form (Beljaars & Holtslag, 1991; Högström, 1988):

$$\psi(\zeta) = \begin{cases} 2\ln(\frac{1+0.95\sqrt{1-11.6\zeta}}{2}) & For\ \zeta < 0 \\ 1 + \left(1+\frac{2}{3}\zeta\right)^{3/2} - \frac{2}{3}(\zeta - 14.3)e^{-0.35\zeta} - 0.95 & For\ \zeta \geq 0 \end{cases} \text{ (S6)}$$

Laminar boundary-layer resistance of quantity $x$ (heat, water, ozone) ($r_{b,x}$) is calculated as (Wesely & Hicks, 1977):

$$r_{b,x} = \frac{2}{ku_*}\left(\frac{D_H}{D_x}\right)^{2/3} \text{ (S7)}$$

Where $D_H$ and $D_x$ are thermal diffusivity and diffusivity of $x$ in air (m$^2$ s$^{-1}$).

**Text S3.**

We roughly estimate the contribution of changes in $v_d$ on surface ozone ($\Delta O_3$) during anomalies by converting the observed and modelled fractional changes ($\Delta v_d/\overline{v_d}$) in midday mean $v_d$:

$$\Delta O_3 = \beta \frac{\Delta v_d}{\overline{v_d}} \quad (S7)$$

$\overline{v_d}$ is taken as the mean of corresponding observed and modelled $v_d$. $\beta$ (ppb, table S1), the sensitivity of surface ozone to $v_d$, is taken from the GEOS-Chem model output from the set of sensitivity simulations performed by Wong et al. (2019), which also gives the details of the model runs. In GEOS-Chem, $v_d$ parameterization is described by Wang et al. (1998), which is essentially a modified form of the Wesely (1989) framework with additional dependence of $r_s$ of on leaf area index (*LAI*) through a simplified canopy radiative transfer equation (Guenther et al., 1995), and linear scaling of cuticular conductance to *LAI*. Input parameters for different land type are publically available (http://wiki.seas.harvard.edu/geos-chem/index.php/Dry_deposition#Input_values_for_dry_deposition). We use summertime (JJA) mean $\beta$ from the model grids that individual sites are located. The monthly variability of $\beta$ is approximately 10% in all the three grids. Furthermore, we partition the expected contribution from stomatal ($\Delta O_{3,s}$) and non-stomatal ($\Delta O_{3,ns}$) pathways by:

$$\Delta O_{3,s} = \Delta O_3 \frac{\Delta g_{s,O_3}}{\Delta g_{ns,O_3} + \Delta g_{s,O_3}} \quad \text{and} \quad \Delta O_{3,ns} = \Delta O_3 \frac{\Delta g_{ns,O_3}}{\Delta g_{ns,O_3} + \Delta g_{s,O_3}} \quad (S8)$$

Where $\Delta g_{s,O3}$ and $\Delta g_{ns,O3}$ are the observed and modelled changes in $g_{s,O3}$, $g_{ns,O3}$ during anomalies. The result is given at fig. S2.
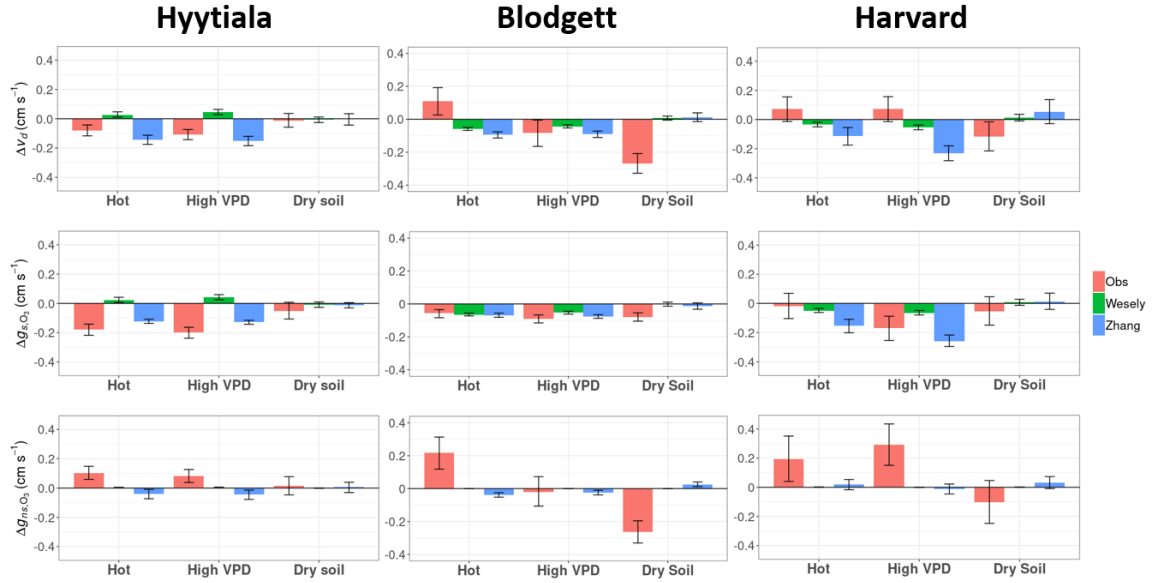
**Figure S1**. Differences in summer midday (9am – 3pm) $v_d$, $g_{s,O3}$ and $g_{ns,O3}$ between abnormal and normal days derived from Penman-Monteith based partitioning. The error bars indicate 95% confidence interval for the differences, while the colors of the bars indicate source of the data (observed, modelled by Wesely or Zhang schemes).

|  | Hyytiälä Forest | Blodgett Forest | Harvard Forest |
|---|---|---|---|
| Latitude, Longitude | 61.85, 24.29 | 38.89, −120.63 | 42.5378, −72.1715 |
| Canopy height (m) | 15 | 8 | 24 |
| Elevation (m) | 181 | 1315 | 340 |
| Mean Annual temperature (°C) | 3.8 | 11.09 | 6.62 |
| Mean Annual Precipitation (mm) | 709 | 1126 | 1071 |
| IGBP land cover type | Evergreen Needleleaf Forest | Evergreen Needleleaf Forest | Deciduous Broadleaf Forest |
| Years of available $O_3$ flux data | 2003 – 2005, 2007 – 2013 | 2001 – 2007 | 1992 – 2000 |
| Years of available soil moisture data | 2003, 2005, 2007 – 2013 | 2001 – 2005 | 1995 – 2000 |
| Peak growing season[*] | Week 25 – 34 | Days 172 – 264 | June 1st – September 15th |
| Peak growing season LAI[#] | 3.5 | 1.2 – 2.9 | 4.4 – 5.2 |
| Available days of observed midday $v_d$ | 501 | 448 | 405 |
| Median (±sd) midday $v_d$ during all available days (cm s$^{-1}$) | 0.59 ± 0.13 | 0.63 ± 0.23 | 0.62 ± 0.28 |
| High $T$ and high $VPD$ overlapping days | 30 | 31 | 14 |
| High $T$ and low $SWC$ overlapping days | 5 | 2 | 6 |
| High $VPD$ and low $SWC$ overlapping days | 5 | 8 | 9 |
| β (ppb) | 13.0 | 8.44 | 13.6 |

**Table S1.** Main characteristics of the sites considered in this study. [*]: Definition of peak growing season are quoted from Rannik et al., (2012) for Hyytiala, Fares et al., (2010) for Blodgett and Clifton et al., (2017) for Harvard. [#]: Data are from Launiainen et al., (2016) for Hyytiala, Fares et al., (2010) for Blodgett and biomass inventory data (HF069) of Harvard Forest Archive for Harvard (Munger and Wofsy, 2020). Interpolation and multi-annual averages are used for Blodgett and Harvard, respectively.

|  | Wesely | Zhang |
|---|---|---|
| $R_s$ | $R_s = r_s(SW_{in})f_T \dfrac{D_{H_2O}}{D_{O_3}}$ | $R_s = \dfrac{r_s(PAR, LAI)}{(1-w_{st})f_T f_{vpd} f_\psi} \dfrac{D_{H_2O}}{D_{O_3}}$ |
| Cuticular Resistance ($R_{cut}$) | $R_{cut} = \dfrac{R_{cut_0}}{LAI}$ | For dry surface, $$R_{cut} = \dfrac{R_{cut_{d0}}}{e^{0.03RH}LAI^{0.25}u_*}$$ For wet surface, $$R_{cut} = \dfrac{R_{cut_{w0}}}{LAI^{0.5}u_*}$$ |
| In-canopy aerodynamic resistance ($R_{ac}$) | Prescribed | $R_{ac} = R_{ac_0} \dfrac{LAI^{0.25}}{u_*}$ |
| Ground Resistance ($R_g$) | Prescribed || 
| Lower-canopy aerodynamic resistance ($R_{alc}$) | $R_{alc} = 100(1 + \dfrac{1000}{SW_{in}+10})$ | - |
| Lower-canopy surface resistance ($R_{clc}$) | Prescribed | - |

**Table S2.** Brief description of the two dry deposition parameterizations. Parameterizations of aerodynamic and laminar boundary-layer resistance are given in text S1, so only components of surface resistance is described. *PAR* = photosynthetically active radiation, $f_T$ = temperature (*T*) stress function, $f_{vpd}$ = *VPD* stress function, $f_\psi$ = leaf water potential (*ψ*) stress function, $w_{st}$ = stomatal blocking fraction, *RH* = relative humidity. The constants for corresponding land types can be found in Wesely (1989) and Zhang et al. (2003). Peak growing season parameters are used for the Wesely model.

**References:**

Beljaars, A. C. M., & Holtslag, A. A. M. (1991). Flux parameterization over land surfaces for atmospheric models. *Journal of Applied Meteorology*, *30*(3), 327–341. https://doi.org/10.1175/1520-0450(1991)030<0327:FPOLSF>2.0.CO;2

Breiman, L. (2001). Random Forrests. *Machine Learning*, *45*(1), 5–32.

Clifton, O. E., Fiore, A. M., Munger, J. W., Malyshev, S., Horowitz, L. W., Shevliakova, E., … Griffin, K. L. (2017). Interannual variability in ozone removal by a temperate deciduous forest. *Geophysical Research Letters*, *44*(1), 542–552. https://doi.org/10.1002/2016GL070923

Ducker, J. A., Holmes, C. D., Keenan, T. F., Fares, S., Goldstein, A. H., Mammarella, I., … Schnell, J. (2018). Synthetic ozone deposition and stomatal uptake at flux tower sites. *Biogeosciences*, *15*(17), 5395–5413. https://doi.org/10.5194/bg-15-5395-2018

Fares, S., McKay, M., Holzinger, R., & Goldstein, A. H. (2010). Ozone fluxes in a Pinus ponderosa ecosystem are dominated by non-stomatal processes: Evidence from long-term continuous measurements. *Agricultural and Forest Meteorology*, *150*(3), 420–431. https://doi.org/10.1016/j.agrformet.2010.01.007

Foken, T. (2006). 50 years of the Monin-Obukhov similarity theory. *Boundary-Layer Meteorology*. https://doi.org/10.1007/s10546-006-9048-6

Gerosa, G., Derghi, F., & Cieslik, S. (2007). Comparison of different algorithms for stomatal ozone flux determination from micrometeorological measurements. *Water, Air, and Soil Pollution*, *179*(1–4), 309–321. https://doi.org/10.1007/s11270-006-9234-7

Guenther, A. B., Hewitt, C. N., Erickson, D., Fall, R., Geron, C., Graedel, T., … Zimmerman, P. (1995). A global model of natural volatile organic compound emissions. *J. Geophys. Res.*, *100*(D5), 8873–8892. https://doi.org/10.1029/94JD02950

Högström, U. (1988). Non-dimensional wind and temperature profiles in the atmospheric surface layer: A re-evaluation. *Boundary-Layer Meteorology*, *42*(1–2), 55–78. https://doi.org/10.1007/BF00119875

Kurpius, M. R., & Goldstein, A. H. (2003). Gas-phase chemistry dominates O3 loss to a forest, implying a source of aerosols and hydroxyl radicals to the atmosphere. *Geophysical Research Letters*. https://doi.org/10.1029/2002GL016785

Launiainen, S., Katul, G. G., Kolari, P., Lindroth, A., Lohila, A., Aurela, M., … Vesala, T. (2016). Do the energy fluxes and surface conductance of boreal coniferous forests in Europe scale with leaf area? *Global Change Biology*. https://doi.org/10.1111/gcb.13497

Monin, A. S., & Obukhov, A. M. (1954). Basic laws of turbulent mixing in the surface layer of the atmosphere. *Contrib. Geophys. Inst. Acad. Sci. USSR*, *24*(151), 163–187.

Nelson, J. A., Carvalhais, N., Cuntz, M., Delpierre, N., Knauer, J., Ogée, J., … Jung, M. (2018). Coupling Water and Carbon Fluxes to Constrain Estimates of Transpiration: The TEA Algorithm. *Journal of Geophysical Research: Biogeosciences*. https://doi.org/10.1029/2018JG004727

Rannik, Ü., Altimir, N., Mammarella, I., Bäck, J., Rinne, J., Ruuskanen, T. M., … Kulmala, M. (2012). Ozone deposition into a boreal forest over a decade of observations: Evaluating deposition partitioning and driving variables. *Atmospheric*

*Chemistry and Physics*, *12*(24), 12165–12182. https://doi.org/10.5194/acp-12-12165-2012

Stoy, P. C., El-Madany, T. S., Fisher, J. B., Gentine, P., Gerken, T., Good, S. P., … Wolf, S. (2019). Reviews and syntheses: Turning the challenges of partitioning ecosystem evaporation and transpiration into opportunities. *Biogeosciences*. https://doi.org/10.5194/bg-16-3747-2019

Wang, Y., Jacob, D. J., & Logan, J. A. (1998). Global simulation of tropospheric O 3-NO x-hydrocarbon chemistry - 1. Model formulation. *Journal of Geophysical Research D: Atmospheres*, *103*(3339), 10713–10725. https://doi.org/10.1029/98jd00158

Wesely, M. L. (1989). Parameterization of surface resistances to gaseous dry deposition in regional-scale numerical models. *Atmospheric Environment*, *41*(SUPPL.), 52–63. https://doi.org/10.1016/j.atmosenv.2007.10.058

Wesely, M. L., & Hicks, B. B. (1977). Some factors that affect the deposition rates of sulfur dioxide and similar gases on vegetation. *Journal of the Air Pollution Control Association*, *27*(11), 1110–1116. https://doi.org/10.1080/00022470.1977.10470534

Wong, A. Y. H., Geddes, J. A., Tai, A. P. K., & Silva, S. J. (2019). Importance of dry deposition parameterization choice in global simulations of surface ozone. *Atmospheric Chemistry and Physics*, *19*(22), 14365–14385. https://doi.org/10.5194/acp-19-14365-2019

Zhang, L., Brook, J. R., & Vet, R. (2003). A revised parameterization for gaseous dry deposition in air-quality models. *Atmospheric Chemistry and Physics*, *3*(6), 2067–2082. https://doi.org/10.5194/acp-3-2067-2003